

(Magneto)Transport Properties of $(\text{TiZrNbNi})_{1-x}\text{Cux}$ and $(\text{TiZrNbCu})_{1-x}\text{Cox}$ Complex Amorphous Alloys

Kuveždić, Marko; Tafra, Emil; Figueroa, Ignacio A.; Basletić, Mario

Source / Izvornik: **Materials**, 2023, 16

Journal article, Published version

Rad u časopisu, Objavljena verzija rada (izdavačev PDF)

<https://doi.org/10.3390/ma16041711>

Permanent link / Trajna poveznica: <https://urn.nsk.hr/urn:nbn:hr:217:584617>

Rights / Prava: [Attribution 4.0 International](#)/[Imenovanje 4.0 međunarodna](#)

Download date / Datum preuzimanja: **2024-11-18**






Repository / Repozitorij:

[Repository of the Faculty of Science - University of Zagreb](#)



Article

(Magneto)Transport Properties of $(\text{TiZrNbNi})_{1-x}\text{Cu}_x$ and $(\text{TiZrNbCu})_{1-x}\text{Co}_x$ Complex Amorphous Alloys

Marko Kuveždić ¹, Emil Tafra ¹, Ignacio A. Figueroa ² and Mario Basletić ^{1,*}¹ Department of Physics, Faculty of Science, University of Zagreb, Bijenička Cesta 32, 10000 Zagreb, Croatia² Instituto de Investigaciones en Materiales, Universidad Nacional Autónoma de México (UNAM), Circuito Exterior s/n, Cd. Universitaria, Ciudad de México 04510, Mexico

* Correspondence: basletic@phy.hr

Abstract: We present a systematic study of electrical resistivity, superconductive transitions and the Hall effect for three systems of compositionally complex amorphous alloys of early (TE) and late (TL) transition metals: $(\text{TiZrNbNi})_{1-x}\text{Cu}_x$ and $(\text{TiZrNbCu})_{1-x}\text{Co}_x$ in a broad composition range of $0 < x < 0.5$ as well as $\text{Ti}_{0.30}\text{Zr}_{0.15}\text{Nb}_{0.15}\text{Cu}_{0.2}\text{Ni}_{0.2}$, $\text{Ti}_{0.15}\text{Zr}_{0.30}\text{Nb}_{0.15}\text{Cu}_{0.2}\text{Ni}_{0.2}$ and $\text{Ti}_{0.15}\text{Zr}_{0.15}\text{Nb}_{0.30}\text{Cu}_{0.2}\text{Ni}_{0.2}$. All samples showed high resistivity at room temperature, 140–240 $\mu\Omega$ cm, and the superconducting transition temperatures decreased with increasing late transition metal content, similar to binary amorphous and crystalline high-entropy TE-TL alloys. The Hall coefficient R_H was temperature-independent and positive for all samples (except for $(\text{TiZrNbCu})_{0.57}\text{Co}_{0.43}$), in good agreement with binary TE-TL alloys. Finally, for the temperature dependence of resistivity, as far as the authors are aware, we present a new model with two conduction channels, one of them being variable range hopping, such as the parallel conduction mode in the temperature range 20–200 K, with the exponent $p = 1/2$. We examine this in the context of variable range hopping in granular metals.

Keywords: compositionally complex alloys; amorphous alloys; metallic glasses; Hall effect; superconductivity; electronic properties; variable range hopping



Citation: Kuveždić, M.; Tafra, E.; Figueroa, I.A.; Basletić, M. (Magneto)Transport Properties of $(\text{TiZrNbNi})_{1-x}\text{Cu}_x$ and $(\text{TiZrNbCu})_{1-x}\text{Co}_x$ Complex Amorphous Alloys. *Materials* **2023**, *16*, 1711. <https://doi.org/10.3390/ma16041711>

Academic Editor: Israel Felner

Received: 26 December 2022

Revised: 9 February 2023

Accepted: 15 February 2023

Published: 18 February 2023



Copyright: © 2023 by the authors. Licensee MDPI, Basel, Switzerland. This article is an open access article distributed under the terms and conditions of the Creative Commons Attribution (CC BY) license (<https://creativecommons.org/licenses/by/4.0/>).

1. Introduction

Over the decades, metallic glass alloys of early (TE) and late (TL) transition elements have been extensively studied [1–3], and the interest further increased after the discovery of TE-TL-base bulk metallic glasses [4]. These alloys are distinguished by a broad range of compositions (typically 20–70% of the TL content) that form metallic glasses [5], which permits detailed systematic studies of the composition dependence of the electronic structure and mechanical and functional properties.

More recently, the development of new materials has shifted from traditional binary and ternary alloys to multicomponent compositionally complex alloys. First employed in an effort to discover new bulk metallic glasses [6,7], this shift soon expanded to crystalline high-entropy alloys [8,9] and eventually to intermetallic compounds and ceramics [10,11]. These new multicomponent metallic glasses offer interesting new research prospects. They allow us to expand our understanding of the effects of composition changes and chemical complexity on material properties, and they open up the possibility of comparisons with high-entropy alloys, which possess chemical but not structural disorder [12–14].

Furthermore, their excellent mechanical properties and phase stability in a large temperature range makes them interesting for technological application, such as magnetocaloric devices [15] and antidiffusion and anticorrosive coatings (see, for example, [16] for a review). Continuing our work on multicomponent compositionally complex metal alloys [17–22], we report here on the results of a systematic study of electronic properties (the electrical resistivity, superconductive transitions and Hall effect) on amorphous samples of two quinary TE-TL alloy systems $(\text{TiZrNbNi})_{1-x}\text{Cu}_x$ and $(\text{TiZrNbCu})_{1-x}\text{Co}_x$ (from hereon Cu_x and Co_x , respectively).

Additionally, we report on a set of thin ribbons prepared with the same procedures with nominal compositions: $\text{Ti}_{0.30}\text{Zr}_{0.15}\text{Nb}_{0.15}\text{Cu}_{0.2}\text{Ni}_{0.2}$, $\text{Ti}_{0.15}\text{Zr}_{0.30}\text{Nb}_{0.15}\text{Cu}_{0.2}\text{Ni}_{0.2}$ and $\text{Ti}_{0.15}\text{Zr}_{0.15}\text{Nb}_{0.30}\text{Cu}_{0.2}\text{Ni}_{0.2}$ (from hereon $\text{Ti}_{0.30}$, $\text{Zr}_{0.30}$ and $\text{Nb}_{0.30}$, respectively). These alloys possess varying concentrations of TE elements while maintaining the same ratio of TE to TL as $(\text{TiZrNb})_{0.6}(\text{NiCu})_{0.4}$ (the same composition as $\text{Cu}_{0.20}$ and $\text{Ni}_{0.20}$). We compare our results to similar binary TE-TL metallic glass alloys.

Lastly, we propose an explanation of the negative temperature coefficient of the temperature dependence of the resistivity, a long-standing issue for an entire class of strong scattering amorphous alloys, which we feel is still not solved in a satisfactory way. Our proposition of the observed temperature dependence of resistivity is based on two parallel conducting channels, one being metallic-like and the other similar to variable range hopping (VRH). We show that this surprising appearance of VRH is reminiscent of the VRH in granular metals.

2. Experimental Details

Ingots of Cu_x and Co_x alloys were prepared from high-purity components (≥ 99.8 at.%) by arc melting in high-purity argon in the presence of a titanium getter. From these ingots, thin ribbons of seven different compositions of Cu_x ($x = 0.0, 0.12, 0.20, 0.25, 0.32, 0.43$ and 0.50) and five of Co_x ($x = 0.10, 0.20, 0.25, 0.32$ and 0.43) were fabricated by melt-spinning molten alloys on the surface of a copper roller in a pure He atmosphere. A detailed description of the preparation and results of structural (X-ray powder diffraction—XRD), chemical (scanning electron microscopy with energy dispersive spectroscopy—SEM/EDS) and thermal (differential scanning calorimetry—DSC) characterisation of these ribbons was reported previously [20,22]. XRD and DSC results revealed that all samples except for $\text{Cu}_{0.0}$ were fully amorphous. The SEM/EDS images confirmed a random distribution of constituent elements down to a micrometer scale, and the calculated average concentrations were within 1 at.% of nominal.

This paper describes the structural, chemical and thermal properties; susceptibility; microhardness; and ultraviolet photoemission spectroscopy (UPS) of $\text{Ti}_{0.30}$, $\text{Zr}_{0.30}$ and $\text{Nb}_{0.30}$ [23]. From these measurements, $\text{Ti}_{0.30}$ and $\text{Zr}_{0.30}$ appear fully amorphous, while a study of the structure factors using high-energy XRD (HEXRD) revealed a minor nanocrystalline phase in the amorphous matrix of $\text{Nb}_{0.30}$.

Ribbon samples that were typically 6–8 mm long, 1–2 mm wide and ~ 30 μm thick were mounted on a sample holder with “GE” varnish. Prior to mounting, the samples were thoroughly cleaned in an ultrasonic bath with acetone and isopropyl alcohol. The current and voltage wires were glued with silver paste onto the samples. The silver paste was allowed to dry at room temperature resulting in contact resistances up to 100 Ω . The voltage noise due to contact resistance was negligible compared to the full voltage across the sample in the case of resistance measurements but presented a significant component of small Hall voltage. Uncertainty due to this noise was incorporated in the error values of the Hall coefficient.

The thickness of the ribbon samples was determined from the sample mass, broad surface area and density (determined from the rule of mixtures [17]). Uncertainty due to the finite width of silver paste contacts and the error in determining the sample dimensions (width and thickness) were also considered when calculating the errors of absolute resistivity and the Hall coefficient as well as values derived from those.

The resistance and Hall effect measurements were performed in the variable temperature insert of a 16/18 T Oxford superconducting magnet system in the 1.3–300 K temperature range and in magnetic fields up to ± 16 T. Low-temperature measurements down to 300 mK were performed in a He^3 insert (Heliox, Oxford Instruments, Abingdon, United Kingdom) of the same magnet system. The temperature was measured by a LakeShore 340 Temperature Controller with a calibrated Cernox thermometer situated close to the samples.

Low-temperature superconducting transition measurements were performed with the low frequency (22 Hz) AC method with rms currents in the 20–200 μA range, while the resistance and Hall effect measurements, depending on the sample, were performed with either the low frequency AC or DC method with currents in the 200 μA –2 mA range. For both measurement methods, AC and DC, the current source was Keithley 6221, while the voltages were measured using dual-phase Signal Recovery 5210 and 7225 Lock-in amplifiers and Keithley 2182A nanovolmeters for the AC and DC methods, respectively. The magnetic field was oriented perpendicular to the broad surface of the ribbon samples and to the current direction.

3. Results and Discussion

3.1. Room Temperature Resistivity and Hall Effect

Figure 1a shows the room temperature resistivities of all studied amorphous alloys and their dependence on composition. All measured samples showed a high resistivity at room temperature (140–240 $\mu\Omega\text{ cm}$), as is usual for amorphous TE-TL alloys [24–32], and a small negative temperature coefficient of resistivity in agreement with the Mooij correlation [32,33]. The room temperature resistivities ρ_{RT} exhibited a certain amount of scatter between different samples of nominally the same composition with the error typically no more than around 5%.

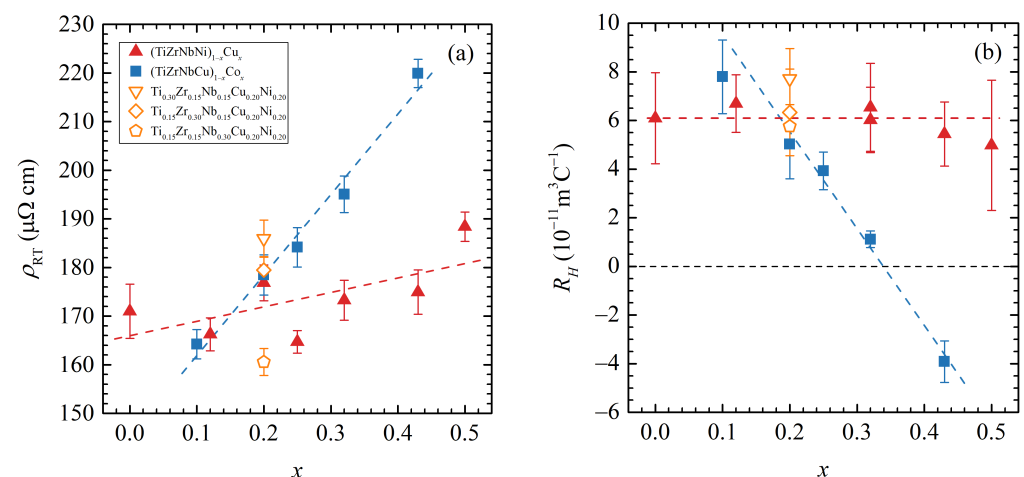


Figure 1. The composition x dependence of the room temperature resistivity ρ_{RT} (a) and Hall constant R_H (b) for (TiZrNbNi) $_{1-x}$ Cu $_x$ (red triangles), (TiZrNbCu) $_{1-x}$ Co $_x$ (blue squares) and three additional alloys with fixed (CuNi) content (open triangles, diamonds and pentagons). The dashed lines are guides to the eye.

For Cu $_x$ alloys, the room temperature resistivities showed a tendency to increase slightly with increasing Cu content with both values and behaviour typical of binary TE-TL alloys [30,31] and similar to the (TiZrNbCu) $_{1-x}$ Ni $_x$ [21] alloys.

On the other hand, for Co $_x$ alloys, the resistivity increased significantly with increasing Co content. This is distinct from binary Zr $_{1-x}$ Co $_x$ alloys which showed a smaller increase from 162 $\mu\Omega\text{ cm}$ for $x = 0.20$ to 183.5 $\mu\Omega\text{ cm}$ for $x = 0.45$ [27], and the difference is likely connected to the presence of Ti, Nb and Cu in our alloys. While it has been suggested [30] that increased $s - d$ scattering is responsible for the increase in resistivity as one approaches the middle of the TE $_{1-x}$ TL $_x$ phase diagram, it is unclear what roles the chemical composition and complexity have on the values of resistivity and the rate of increase with increasing TL content. Further study of more alloys (notably, Ti $_{1-x}$ Co $_x$ and Nb $_{1-x}$ Co $_x$) is needed to build a better understanding of the above-mentioned differences.

The last three alloys studied, with fixed (CuNi) content, showed a small resistivity decrease when going from Ti $_{0.30}$ to Zr $_{0.30}$ and then to Nb $_{0.30}$, which is consistent with the resistivity changes found between binary alloys Ti $_{1-x}$ Ni $_x$, Ti $_{1-x}$ Cu $_x$, Zr $_{1-x}$ Ni $_x$ and

$Zr_{1-x}Cu_x$ and $Nb_{1-x}Ni_x$ (see [29–31] for data on some of those compounds and [32] for a general review on a number of various alloys).

The Hall voltage of all measured samples was linear with the magnetic field and essentially temperature-independent down to the lowest measured temperatures. The calculated values of Hall coefficient R_H were positive—except for $Co_{0.43}$. The Hall coefficient dependence on composition is shown in Figure 1b. R_H drops rapidly for Co_x alloys with increasing Co content with an interpolated critical concentration (the concentration where R_H changes sign) at $x_c = 0.34$. In contrast, Cu_x alloys are generally constant in the measured range of the Cu concentration. Both results are in good agreement with binary TE-TL alloys: the $Zr_{1-x}Co_x$ exhibit a sharp drop with increasing Co content and a critical concentration of $x_c = 0.32$ [34,35], and R_H of $Zr_{1-x}Cu_x$, $Ti_{1-x}Cu_x$. $Hf_{1-x}Cu_x$ amorphous alloys stays mostly constant up to 50% Cu content with a critical concentration around $x_c = 0.8$ [31,35,36].

As for the alloys with a fixed (CuNi) content, they are similar to the binary TE-Cu alloys where the R_H also decreases when going from Ti to Zr and Nb [30,31]. The large change in R_H values in Co_x alloys is consistent with a strong increase and a shift towards the Fermi level of the peak corresponding to the 3D state of Co in the UPS spectra [22]. On the other hand, the peak associated with the 3D states of Cu, which sits further from the Fermi level, shifts only slightly with increasing Cu content [20], which we associate with the nearly constant R_H values in Cu_x alloys.

3.2. Superconductivity

All our samples, except for $Cu_{0.50}$ and $Co_{0.43}$, were superconducting above 300 mK. Variation of the superconducting transition temperatures T_c , defined as the temperature at which the resistivity drops to half the normal resistivity right above the transitions $\rho(T_c) = 0.5\rho_N$, with composition can be found in Figure 2a. The width of the resistive transitions ΔT_c varied between 0.4 K for $Co_{0.20}$ and 0.04 K for $Ti_{0.30}$, where ΔT_c is defined as the temperature interval between $0.1\rho_N$ and $0.9\rho_N$. As previously noted [21], the T_c s values are lower than one would expect for binary alloys of similar composition.

On the other hand, the monotonic decrease of T_c with increasing TL content, with the exception of $Cu_{0.0}$, is consistent with other amorphous [21,27,37–39] and crystalline [40,41] TE-TL alloys. The $Cu_{0.0}$ sample was noted for containing small amounts of a nanocrystalline phase in the amorphous matrix [20], which could affect its results. Furthermore, a lower value of T_c for $Ti_{0.30}$ compared to $Zr_{0.30}$ and $Nb_{0.30}$ is consistent with measurements on $(Zr_{1-x}Ti_x)_{0.78}Ni_{0.22}$ and $(Zr_{1-x}Nb_x)_{0.78}Ni_{0.22}$ [39], which showed a significant decrease of T_c with increasing Ti content, while increasing the Nb content first increased and then decreased T_c values.

The above-mentioned analogous behaviour of T_c with TL content in both our and the binary amorphous TE-TL alloys strongly suggests that the same underlying mechanism is responsible for the suppression of T_c in these systems. It has been argued that the change of T_c with composition in TE-TL is primarily due to changes in the split-band structure of the density of states, which is seen in the UPS spectra [19,21,39]. However, a full understanding of T_c dependence on alloy content is still lacking, and further research is needed on a wider range of different amorphous systems.

In Figure 2b, we present the temperature dependence of the normalized resistivity $\rho(T)/\rho_N$ in the vicinity of the superconducting transition for a $Cu_{0.20}$ sample in a magnetic field. With an increasing magnetic field, the transition temperature T_c drops, and the transition width increases, with the broadening becoming stronger as the temperature decreases. Therefore, to avoid the effects of this broadening, when determining the transition temperatures at different magnetic fields $T_c(\mu_0H)$, we opted to use a different resistivity criteria $\rho(T_c(\mu_0H)) = 0.9\rho_N$. From these measurements, we then determined the temperature dependence of the upper critical fields $\mu_0H_{c2}(T)$, which are shown in Figure 2d–f. The lines on these figures represent the initial slopes of the upper critical field $(\mu_0 dH_{c2}/dT)_{T=T_c}$.

The absolute values of the initial slopes decrease for Cu_x samples from 2.6 TK^{-1} to 2.3 TK^{-1} and increase for Co_x samples from 2.7 TK^{-1} to 3.2 TK^{-1} (except for the $\text{Co}_{0.20}$ sample, which had a value around 2.5 TK^{-1}). The $\text{Ti}_{0.30}$ slope at 2.7 TK^{-1} was somewhat higher than that of $\text{Zr}_{0.30}$ at 2.5 TK^{-1} and $\text{Nb}_{0.30}$ at 2.4 TK^{-1} .

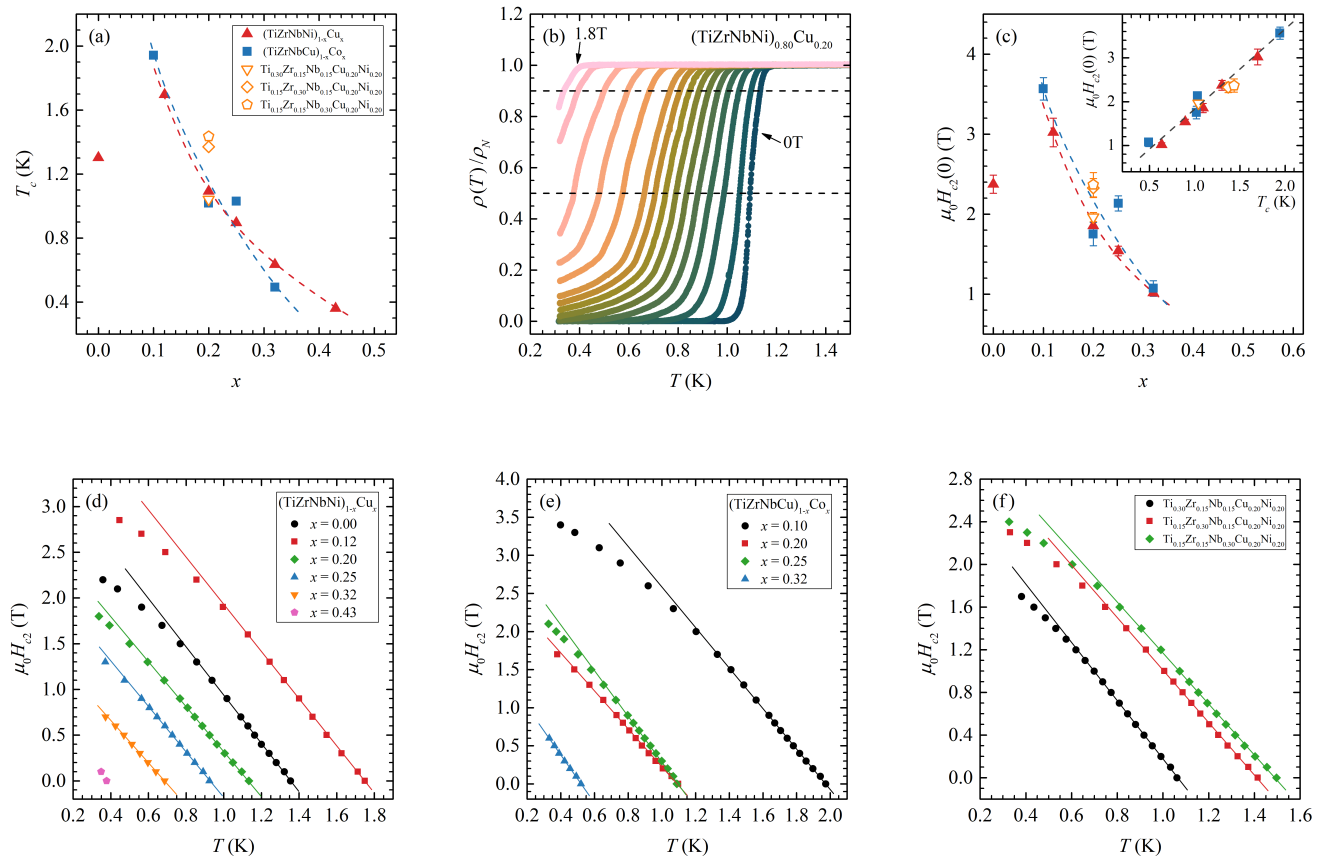


Figure 2. (a) The composition x dependence of the superconducting transition temperatures T_c for $(\text{TiZrNbNi})_{1-x}\text{Cu}_x$ (red triangles), $(\text{TiZrNbCu})_{1-x}\text{Co}_x$ (blue squares) and three additional alloys with fixed (CuNi) content (open triangles, diamonds and pentagons). The dashed lines are guides to the eye. (b) The temperature dependence of the normalized resistivity $\rho(T)/\rho_N$ close to the superconducting transition for the $\text{Cu}_{0.20}$ sample in constant magnetic fields from 0–1.8T. (c) The composition x dependence of the upper critical fields at zero temperature $\mu_0 H_{c2}(0)$ (see panel (a) for details). Inset: $\mu_0 H_{c2}(0)$ vs. T_c for all samples; the dashed line corresponds to the Pauli paramagnetic limit $\mu_0 H_{c2}^{\text{Pauli}} = 1.83T_c$. (d–f) The temperature dependence of the upper critical fields $\mu_0 H_{c2}(T)$ for $(\text{TiZrNbNi})_{1-x}\text{Cu}_x$, $(\text{TiZrNbCu})_{1-x}\text{Co}_x$ and three additional alloys with fixed (CuNi) content. The lines represent the initial slopes of the upper critical field $(\mu_0 dH_{c2}/dT)_{T=T_c}$.

From these slopes, we can estimate the upper critical fields at zero temperature using the Werthamer–Helfand–Hohenberg (WHH) approximation in the dirty limit [42]:

$$\mu_0 H_{c2}(0) = -0.69T_c \left(\mu_0 \frac{dH_{c2}}{dT} \right)_{T=T_c}, \quad (1)$$

as shown in Figure 2c. The $\mu_0 H_{c2}(0)$ values for all samples are close to the Pauli paramagnetic limit $\mu_0 H_{c2}^{\text{Pauli}} = 1.83T_c$ (see inset of Figure 2c), which indicates that superconductivity is destroyed by paramagnetic pair breaking when the Zeeman energy becomes comparable to the superconducting gap energy.

3.3. Temperature Dependence of Resistivity

A small negative temperature coefficient of resistivity for strong scattering amorphous alloys ($\geq 150 \mu\Omega \text{ cm}$) is a long-standing issue; for a detailed discussion, see, for example, [32]. For amorphous alloys at temperatures $\gtrsim 30 \text{ K}$, it is argued [25,26,32,43] that the temperature dependence of conductivity primarily arises from weak localization—specifically from the temperature variation of the inelastic scattering time τ_i . When electron–phonon interactions are the dominant contribution to τ_i —a reasonable assumption for amorphous metals—two temperature dependence regimes appear: $\sigma \sim \sqrt{T}$ for $T > \Theta_D$ and $\sigma \sim T$ for $T < \Theta_D$. We previously analysed the resistivity data for Ni_x alloys and found reasonably good agreement with these temperature variations above and below 100 K [21].

While the resistivity of our alloys presented here shows similar temperature behaviour, we suggest another origin for the observed $\rho(T)$ temperature dependence: we argue that the total resistivity can be described by two parallel conductance channels in the form of:

$$1/\rho(T) = 1/\rho_{\text{Metal}}(T) + 1/\rho_{\text{VRH}}(T). \quad (2)$$

The $\rho_{\text{Metal}}(T)$ is expected to be an ordinary metallic-like contribution. As our systems are disordered ones, we expect it to have a nearly constant value ρ_0 at higher temperatures. The second term, $\rho_{\text{VRH}}(T)$, is another contribution, which we argue is of the variable range hopping origin. Figure 3 shows the result of fitting our $\rho(T)$ data for the $\text{Cu}_{0.32}$ alloy to Equation (2). (From here on: points denote measured/calculated data, and lines are fitting curves.) The top left panel (a) shows the overall raw measured data with the fitting curve. The top right panel (b) shows the normalized metallic contribution $\rho_{\text{Metal}}(T)/\rho_{\text{RT}}$ calculated with the fitting procedure. As expected, in the high temperature range, from around 20 to 200 K , we have a temperature-independent contribution.

Although it seems that this behaviour breaks at temperatures above 200 K , we propose that this is likely a consequence of very small variations of the overall resistivity in this temperature range, where a small error in the measured data can have a seemingly large effect (for example, the influence of extrinsic effects on resistance data, such as contact deterioration and thermal expansion of the sample, become significant compared to the VRH-like contribution, which, at room temperature, changes the total resistivity by only 3–5% from the constant ρ_0 value). Therefore, we argue that a temperature-independent $\rho_{\text{Metal}}(T)$ should extend above $T \gtrsim 200 \text{ K}$.

After subtraction of the $\rho_{\text{Metal}}(T)$ from the measured $\rho(T)$, we are left with $\rho_{\text{VRH}}(T)$, which is shown on the bottom right panel (d) of Figure 3 as the temperature dependence of $\rho_{\text{VRH}}(T)/\rho_{\text{RT}}$. It is worth noting that the VRH contribution to the overall $\rho(T)$ is rather small, as its values are 20–30 times larger than $\rho_{\text{Metal}}(T)$ at room temperature. From the plot, it is clear that $\rho_{\text{VRH}}(T)$ can be described by a VRH-like temperature dependence

$$\rho_{\text{VRH}}(T) = \rho_{\text{VRH},0} \exp\left(\frac{T_{\text{VRH}}}{T}\right)^p, \quad (3)$$

with exponent $p = 1/2$, for $T \gtrsim 20 \text{ K}$. (The T_{VRH} and $\rho_{\text{VRH},0}$ are fitting parameters). Although here, we have set $p = 1/2$ by hand, this exponent can be extracted independently using a so-called ‘special logarithmic derivative’ (see, for example, [44,45]), where one calculates:

$$W = -\frac{d(\ln \rho_{\text{VRH}})}{d(\ln T)} = p \left(\frac{T_{\text{VRH}}}{T}\right)^p, \quad (4)$$

and then the slope of the $\ln(W) - \ln(T)$ plot gives the value of p . This is shown on the bottom left panel (c) of Figure 3, where we again unequivocally obtain $p = 1/2$ for $T \gtrsim 20 \text{ K}$. Here, we emphasize that the above fitting procedure is unique in a sense that only one choice of the $\rho_{\text{Metal}}(T)$ values give VRH behaviour for $\rho_{\text{VRH}}(T)$ with unique $p = 1/2$.

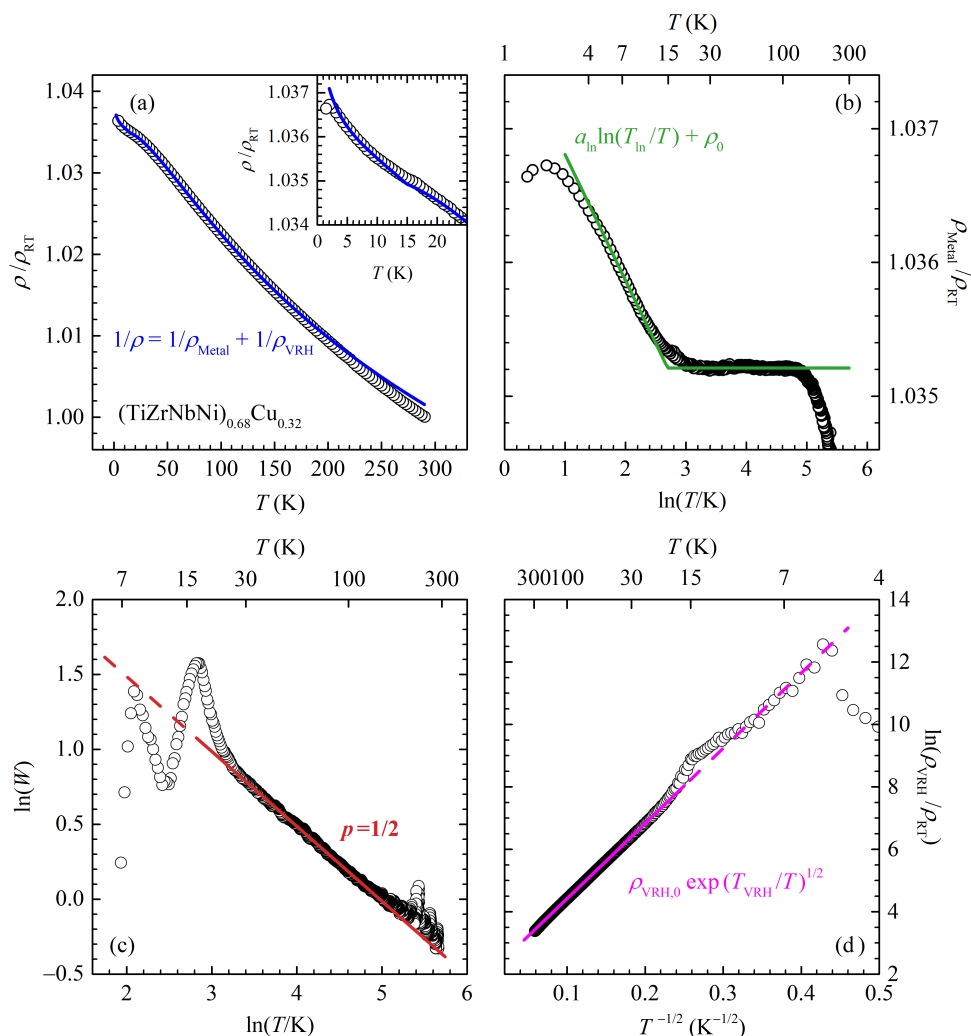


Figure 3. The results of fitting the measured temperature dependence of the $\text{Cu}_{0.32}$ alloy resistivity to the model with two parallel conductance channels. The points are measured data, and the lines are fits. See the text for details. (a) The temperature dependence of the normalized resistivity ρ/ρ_{RT} . Inset: low-temperature detail of the main panel. (b) The temperature dependence of the metallic part $\rho_{\text{Metal}}(T)/\rho_{RT}$. (c) The ‘special logarithmic derivative’ plot of the VRH-like contribution of the resistivity (see Equation (4)) with a $p = 1/2$ slope. (d) Plot of the VRH-like contribution $\ln(\rho_{\text{VRH}}/\rho_{RT})$ vs. $1/\sqrt{T}$.

The described fitting procedure can be satisfactorily applied to all our alloys, Cu_x , Co_x and alloys with a fixed (CuNi) content, resulting in consistent values of fitting parameters. In addition, we reanalysed the resistivity data for Ni_x as previously reported in [21]. Figure 4 shows the fitting parameters $\rho_{\text{VRH}}(T)$ (a), a_{\ln} (b) and T_{\ln} panel (c) dependence on the studied alloys (concentration). T_{VRH} is virtually constant for all alloys, except for Co_x , which suggests a linear increase with Co concentration. a_{\ln} is around $0.15 \mu\Omega \text{ cm}$, and T_{\ln} is around 15 K; in our opinion, this indicates that the entire idea of two parallel conducting channels, one being ‘metallic’ and other VRH-like, might be physically sound.

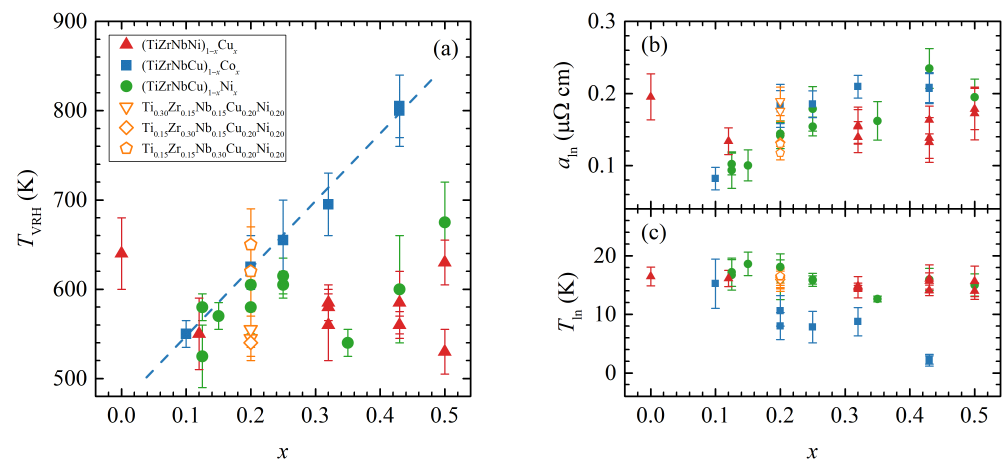


Figure 4. (a–c) The composition x dependence of the fitting parameters T_{VRH} , a_{in} and T_{in} , respectively, for $(\text{TiZrNbNi})_{1-x}\text{Cu}_x$ (red triangles), $(\text{TiZrNbCu})_{1-x}\text{Co}_x$ (blue squares), $(\text{TiZrNbCu})_{1-x}\text{Ni}_x$ (green circles) and three additional alloys with fixed (CuNi) content (open triangles, diamonds and pentagons). The dashed line is a guide to the eye. Multiple points for the same x correspond to multiple measured samples.

From the physical standpoint, the metallic contribution of the conductivity is clear. However, the origin of this VRH-like conduction mode and particularly the $p = 1/2$ exponent is not immediately apparent. In a rather simple picture, localized states formed due to Anderson localization (driven by chemical and structural disorder), form randomly distributed insulating regions throughout the sample. These insulating regions then contribute to the VRH conductivity channel in the observed temperature dependence of resistivity.

It is well-known that the Anderson localization can lead to either a Mott [46] or an Efros–Shklovskii VRH mechanism [47]. In Mott VRH, the exponent p is dependent on the underlying system dimensionality and, for 3D systems, should be $p = 1/4$, while the value we found, $p = 1/2$, is characteristic for 1D systems, which clearly is not the case (our alloys are 3D). On the other hand, the Efros–Shklovskii VRH formalism appears more promising as it predicts a $p = 1/2$ exponent irrespective of the dimensionality of the system. However, the temperature range (>20 K) in which we have a VRH-like conduction mode is higher than temperatures where this mechanism is usually observed (on the order of 10 K or less) [47,48].

A VRH-like temperature dependence in resistivity and a $p = 1/2$ exponent were also obtained in granular metals (composite materials of conductive metallic regions embedded in an insulating matrix). In these systems, the hopping occurs between isolated metallic regions, which results in single carrier charging of those regions and an associated Coulomb penalty that results in the $p = 1/2$ exponent—similar to the Efros–Shklovskii formalism but on a larger distance scale (see [49,50] for experimental details and [48,51] for theoretical considerations).

We propose that this is similar to our alloys: while delocalised states form an infinite cluster, the random spatial distribution of the aforementioned localised states (insulating regions) results in the appearance of finite clusters (isolated pockets) as well as dead ends (blind alleys) (see Figure 5), which do not contribute to the metallic conductivity, simultaneously increasing the resistivity [47]. Such isolated pockets and blind alleys could act as metallic regions in granular metals with localised states acting as the insulating regions. Hopping between these features could then result in a VRH-like conduction mode, parallel to the metallic conduction in the infinite cluster.

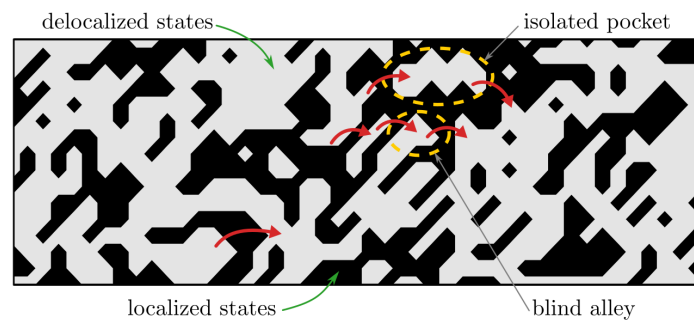


Figure 5. Illustration of the origin of the variable range hopping conductance contribution (see text for details). Gray area: the conductive region, corresponding to the delocalized states. Black area: nonconductive region due to the localization (driven by chemical and structural disorder). Red arrows: hopping between isolated pockets and/or blind alleys.

Furthermore, in the granular metal theory of VRH, T_{VRH} is dependent on the dielectric constant of the insulating region and, more importantly, on the (volume) ratio of the insulating and metallic regions [49]. This would indicate that the observed T_{VRH} increase with Co content in our Co_x alloys could be the result of an increase of the ratio of localised to delocalized states, which is, in turn, consistent with the increase of ρ_{RT} with Co content.

Finally, it is interesting to note increasing $\rho_{\text{Metal}}(T)$ for temperatures below 20 K; see the top right panel (b) of Figure 3. One can argue that this temperature dependence is proportional to $\ln T$, which is often found in metallic glass alloys. Several suggestions have been proposed to explain this resistivity behaviour in those systems, for example, the Kondo effect ($\sim \ln T$), scattering from two-level tunnelling states ($\sim \ln T$ or $\sim T$) and electron–electron interaction effects ($\sim T$) [32]. However, since the low-temperature resistivity ($T \lesssim 20$ K) of our samples could be equally well-fitted to a \sqrt{T} dependence with a similar qualitative behaviour of corresponding fitting parameters, we feel that more work and results from other experimental techniques are required for a better understanding.

4. Conclusions

In this manuscript, the results of a systematic study of electrical resistivity, superconductive transitions and the Hall effect of amorphous samples of two quinary TE-TL alloy systems $(\text{TiZrNbNi})_{1-x}\text{Cu}_x$ and $(\text{TiZrNbCu})_{1-x}\text{Co}_x$ and three samples with the nominal compositions $\text{Ti}_{0.30}\text{Zr}_{0.15}\text{Nb}_{0.15}\text{Cu}_{0.2}\text{Ni}_{0.2}$, $\text{Ti}_{0.15}\text{Zr}_{0.30}\text{Nb}_{0.15}\text{Cu}_{0.2}\text{Ni}_{0.2}$ and $\text{Ti}_{0.15}\text{Zr}_{0.15}\text{Nb}_{0.30}\text{Cu}_{0.2}\text{Ni}_{0.2}$ in the temperature range of 0.3–300 K and in magnetic fields up to ± 16 T are presented and compared to those of binary and multicomponent TE-TL alloys.

All measured samples showed a high resistivity at room temperature (140–240 $\mu\Omega$ cm) and a small negative temperature coefficient of resistivity—both of which are in agreement with binary TE-TL alloys. The dependence of room temperature resistivities ρ_{RT} on composition x is similar to those for corresponding binary alloys, except for Co_x alloys, where the resistivity increase with Co content is more significant than in binary $\text{Zr}_{1-x}\text{Co}_x$ alloys. The results of the Hall effect measurements are in good agreement with binary TE-TL amorphous alloys. The measured Hall coefficient R_H is temperature-independent and positive (except for $\text{Cu}_{0.43}$). With the change in composition x , R_H is nearly constant for Cu_x alloys, while, for Co_x alloys, R_H decreases with increasing Co content and changes sign around $x(\text{Co}) = 0.34$.

These changes, or lack thereof, are consistent with the shift in position of the peaks associated with 3D states of Cu and Co in the UPS spectra. Furthermore, for alloys with fixed (CuNi) content, R_H increases with additional Ti content and decreases with additional Zr or Nb content. The observed superconducting transition temperatures T_c are surprisingly low ($T_c \leq 1.94$ K) and decrease further with increasing TL (Cu and Co) content—the latter being consistent with other amorphous and crystalline TE-TL alloys. The upper critical fields at zero temperature $\mu_0 H_{c2}(0)$ appear to be Pauli limited.

As for the temperature dependence of the resistivity—in particular, its increase with decreasing temperature—we present a model with two parallel conductance channels in the form $1/\rho(T) = 1/\rho_{\text{Metal}}(T) + 1/\rho_{\text{VRH}}(T)$ and show that, for $T \gtrsim 20$ K, our data can be nicely fitted with a constant $\rho_{\text{Metal}}(T)$ and variable range hopping, such as contribution $\rho_{\text{VRH}}(T)$ with exponent $p = 1/2$. From a physical standpoint, the temperature-independent $\rho_{\text{Metal}}(T)$ agrees with the notion that the system is strongly disordered.

For the origin of $\rho_{\text{VRH}}(T)$, we propose the idea that a portion of states near the Fermi level are localized due to the disorder, resulting in insulating and conductive metallic regions. The random spatial distribution of these localised states (insulating regions) throughout the samples creates isolated pockets and blind alleys, which do not contribute to the metallic conductivity but contribute to conductivity via a hopping mechanism akin to VRH in granular metals.

To conclude, we propose that measurements on amorphous thin films of varying thickness of these (Ti-Zr-Nb-Ni-Cu and Ti-Zr-Nb-Co-Ni) and similar alloys could provide further insight into the nature of the possible VRH regime that we observed in our alloys.

Author Contributions: Methodology, I.A.F. and M.K.; Investigation, M.K.; Resources, E.T. and M.B.; Writing—original draft, M.K. and M.B.; Writing—review & editing, M.B. and M.K. All authors have read and agreed to the published version of the manuscript.

Funding: This work was partially supported by the Croatian Science Foundation Projects No. IP-2018 01-7828. We also acknowledge the support of project CeNIKS co-financed by the Croatian Government and the European Union through the European Regional Development Fund, Competitiveness and Cohesion Operational Programme (Grant no. KK.01.1.1.02.0013). Financial support from the University of Zagreb through funds for multipurpose institutional financing of scientific research (project 104-20286446) is greatly acknowledged.

Institutional Review Board Statement: Not applicable.

Informed Consent Statement: Not applicable.

Data Availability Statement: The data presented in the figures are available on request from the M.K. and M.B.

Acknowledgments: We thank E. Babić for the useful discussion and reading of the manuscript.

Conflicts of Interest: The authors declare no conflict of interest. The funders had no role in the design of the study; in the collection, analyses, or interpretation of data; in the writing of the manuscript; nor in the decision to publish the results.

References

1. Güntherodt, H.J.; Beck, H. (Eds.) *Glassy Metals I*; Topics in Applied Physics; Springer: Berlin/Heidelberg, Germany, 1981; Volume 46. [[CrossRef](#)]
2. Beck, H.; Güntherodt, H.J. (Eds.) *Glassy Metal II*; Topics in Applied Physics; Springer: Berlin/Heidelberg, Germany, 1983; Volume 53. [[CrossRef](#)]
3. Beck, H.; Güntherodt, H.J. (Eds.) *Glassy Metals III*; Topics in Applied Physics; Springer: Berlin/Heidelberg, Germany, 1994; Volume 72. [[CrossRef](#)]
4. Inoue, A.; Zhang, W.; Zhang, T.; Kurosaka, K. High-Strength Cu-based Bulk Glassy Alloys in Cu–Zr–Ti and Cu–Hf–Ti Ternary Systems. *Acta Mater.* **2001**, *49*, 2645–2652. [[CrossRef](#)]
5. Buschow, K.H.J. Short-Range Order and Thermal Stability in Amorphous Alloys. *J. Phys. F Met. Phys.* **1984**, *14*, 593. [[CrossRef](#)]
6. Cantor, B.; Kim, K.B.; Warren, P.J. Novel Multicomponent Amorphous Alloys. *Mater. Sci. Forum* **2002**, *386–388*, 27–32. [[CrossRef](#)]
7. Ma, L.; Wang, L.; Zhang, T.; Inoue, A. Bulk Glass Formation of Ti-Zr-Hf-Cu-M (M=Fe, Co, Ni) Alloys. *Mater. Trans.* **2002**, *43*, 277–280. [[CrossRef](#)]
8. Cantor, B.; Chang, I.T.H.; Knight, P.; Vincent, A.J.B. Microstructural Development in Equiatomic Multicomponent Alloys. *Mater. Sci. Eng. A* **2004**, *375–377*, 213–218. [[CrossRef](#)]
9. Yeh, J.W.; Chen, S.K.; Lin, S.J.; Gan, J.Y.; Chin, T.S.; Shun, T.T.; Tsau, C.H.; Chang, S.Y. Nanostructured High-Entropy Alloys with Multiple Principal Elements: Novel Alloy Design Concepts and Outcomes. *Adv. Eng. Mater.* **2004**, *6*, 299–303. [[CrossRef](#)]
10. Gao, M.C.; Yeh, J.W.; Liaw, P.K.; Zhang, Y. (Eds.) *High-Entropy Alloys*; Springer International Publishing: Cham, Switzerland, 2016. [[CrossRef](#)]

11. Murty, B.S.; Yeh, J.W.; Ranganathan, S.; Bhattacharjee, P.P. *High-Entropy Alloys*, 2nd ed.; Elsevier: Amsterdam, The Netherlands; Cambridge, MA, USA, 2019.
12. Babić, E.; Drobac, Đ.; Figueroa, I.A.; Laurent-Brocq, M.; Marohnić, Ž.; Mikšić Trontl, V.; Pajić, D.; Perrière, L.; Pervan, P.; Remenyi, G.; et al. Transition from High-Entropy to Conventional Alloys: Which Are Better? *Materials* **2021**, *14*, 5824. [[CrossRef](#)]
13. Nagase, T.; Takeuchi, A.; Amiya, K.; Egami, T. Solid State Amorphization of Metastable Al_{0.5}TiZrPdCuNi High Entropy Alloy Investigated by High Voltage Electron Microscopy. *Mater. Chem. Phys.* **2018**, *210*, 291–300. [[CrossRef](#)]
14. Meng, Y.H.; Duan, F.H.; Pan, J.; Li, Y. Phase Stability of B2-ordered ZrTiHfCuNiFe High Entropy Alloy. *Intermetallics* **2019**, *111*, 106515. [[CrossRef](#)]
15. Yin, H.; Law, J.Y.; Huang, Y.; Shen, H.; Jiang, S.; Guo, S.; Franco, V.; Sun, J. Enhancing the Magnetocaloric Response of High-Entropy Metallic-Glass by Microstructural Control. *Sci. China Mater.* **2022**, *65*, 1134–1142. [[CrossRef](#)]
16. Arshad, M.; Amer, M.; Hayat, Q.; Janik, V.; Zhang, X.; Moradi, M.; Bai, M. High-Entropy Coatings (HEC) for High-Temperature Applications: Materials, Processing, and Properties. *Coatings* **2022**, *12*, 691. [[CrossRef](#)]
17. Biljaković, K.; Remenyi, G.; Figueroa, I.A.; Ristić, R.; Pajić, D.; Kuršumović, A.; Starešinić, D.; Zadro, K.; Babić, E. Electronic Structure and Properties of (TiZrNbCu)_{1-x}Ni_x High Entropy Amorphous Alloys. *J. Alloys Compd.* **2017**, *695*, 2661–2668. [[CrossRef](#)]
18. Figueroa, I.A.; Ristić, R.; Kuršumović, A.; Biljaković, K.; Starešinić, D.; Pajić, D.; Remenyi, G.; Babić, E. Properties of (TiZrNbCu)_{1-x}Ni_x Metallic Glasses. *J. Alloys Compd.* **2018**, *745*, 455–459. [[CrossRef](#)]
19. Babić, E.; Pajić, D.; Zadro, K.; Biljaković, K.; Trontl, V.M.; Pervan, P.; Starešinić, D.; Figueroa, I.A.; Kuršumović, A.; Michalik, Š.; et al. Structure Property Relationship in (TiZrNbCu)_{1-x}Ni_x Metallic Glasses. *J. Mater. Res.* **2018**, *33*, 3170–3183. [[CrossRef](#)]
20. Ristić, R.; Figueroa, I.A.; Lachová, A.; Michalik, Š.; Mikšić Trontl, V.; Pervan, P.; Zadro, K.; Pajić, D.; Babić, E. Transition from High-Entropy to Cu-based (TiZrNbNi)_{1-x}Cu_x Metallic Glasses. *J. Appl. Phys.* **2019**, *126*, 154105. [[CrossRef](#)]
21. Kuveždić, M.; Tafra, E.; Basletić, M.; Ristić, R.; Pervan, P.; Mikšić Trontl, V.; Figueroa, I.A.; Babić, E. Change of Electronic Properties on Transition from High-Entropy to Ni-rich (TiZrNbCu)_{1-x}Ni_x Alloys. *J. Non-Cryst. Solids* **2020**, *531*, 119865. [[CrossRef](#)]
22. Ristić, R.; Figueroa, I.A.; Salčinović Fetić, A.; Zadro, K.; Mikšić Trontl, V.; Pervan, P.; Babić, E. Transition from High-Entropy to Conventional (TiZrNbCu)_{1-x}Co_x Metallic Glasses. *J. Appl. Phys.* **2021**, *130*, 195102. [[CrossRef](#)]
23. Babić, E.; Figueroa, I.A.; Michalik, S.; Mikšić-Trontl, V.; Pervan, P.; Ristić, R.; Salčinović-Fetić, A.; Starešinić, D.; Zadro, K. Influence of early transition metals on properties of Ti-Zr-Nb-Cu-Ni complex glassy alloys. *J. Appl. Phys. manuscript in preparation*.
24. Ristić, R.; Babić, E.; Šaub, K.; Miljak, M. Electrical and Magnetic Properties of Amorphous Zr_{100-x}Cu_x Alloys. *Fizika* **1983**, *15*, 363–373.
25. Šaub, K.; Babić, E.; Ristić, R. Quantum Corrections to Conductivity of Glassy Zr_{100-x}Cu_x Alloys. *Solid State Commun.* **1985**, *53*, 269–272. [[CrossRef](#)]
26. Babić, E.; Šaub, K. Universal Conductivity Variation in Glassy Zr-M Alloys. *Solid State Commun.* **1985**, *56*, 111–115. [[CrossRef](#)]
27. Altounian, Z.; Strom-Olsen, J.O. Superconductivity and Spin Fluctuations in M – Zr metallic glasses (M = Cu, Ni, Co, and Fe). *Phys. Rev. B* **1983**, *27*, 4149–4156. [[CrossRef](#)]
28. Tafra, E.; Basletić, M.; Ristić, R.; Babić, E.; Hamzić, A. Enhanced Superconductivity in Hf-base Metallic Glasses. *J. Phys. Condens. Matter* **2008**, *20*, 425215. [[CrossRef](#)]
29. Gallagher, B.L.; Greig, D. The Thermoelectric Powers and Resistivities of Amorphous Transition Metal Alloys. *J. Phys. F Met. Phys.* **1982**, *12*, 1721. [[CrossRef](#)]
30. Pavuna, D. On the Concentration Dependence of Transport Coefficients in Amorphous Transition Metal Alloys. *Solid State Commun.* **1985**, *54*, 771–774. [[CrossRef](#)]
31. Ristić, R.; Cooper, J.R.; Zadro, K.; Pajić, D.; Ivkov, J.; Babić, E. Ideal Solution Behaviour of Glassy Cu–Ti,Zr,Hf Alloys and Properties of Amorphous Copper. *J. Alloys Compd.* **2015**, *621*, 136–145. [[CrossRef](#)]
32. Howson, M.A.; Gallagher, B.L. The Electron Transport Properties of Metallic Glasses. *Phys. Rep.* **1988**, *170*, 265–324. [[CrossRef](#)]
33. Mooij, J.H. Electrical Conduction in Concentrated Disordered Transition Metal Alloys. *Phys. Status Solidi A* **1973**, *17*, 521–530. [[CrossRef](#)]
34. Ivkov, J.; Babić, E.; Jacobs, R.L. Hall Effect and Electronic Structure of Glassy Zr 3d Alloys. *J. Phys. F Met. Phys.* **1984**, *14*, L53–L57. [[CrossRef](#)]
35. Ivkov, J.; Babić, E. On the Origin of the Positive Hall Coefficient in Disordered TE-TL Alloys. *J. Phys. Condens. Matter* **1990**, *2*, 3891–3896. [[CrossRef](#)]
36. Howson, M.A.; Greig, D.; Gallagher, B.L.; Morgan, G.J. The Hall Coefficients of CuTi and CuHf Amorphous Metal Alloys. *J. Non-Cryst. Solids* **1984**, *61–62*, 1261–1265. [[CrossRef](#)]
37. Babić, E.; Ristić, R.; Miljak, M.; Scott, M.G.; Gregan, G. Superconductivity in Zirconium-Nickel Glasses. *Solid State Commun.* **1981**, *39*, 139–141. [[CrossRef](#)]
38. Samwer, K.v.; Löhneysen, H. Amorphous Superconducting Zr_xCu_{1-x}: Electronic Properties, Stability, and Low-Energy Excitations. *Phys. Rev. B* **1982**, *26*, 107–123. [[CrossRef](#)]
39. Karkut, M.G.; Hake, R.R. Upper Critical Fields and Superconducting Transition Temperatures of Some Zirconium-Base Amorphous Transition-Metal Alloys. *Phys. Rev. B* **1983**, *28*, 1396–1418. [[CrossRef](#)]
40. Stolze, K.; Tao, J.; von Rohr, F.O.; Kong, T.; Cava, R.J. Sc–Zr–Nb–Rh–Pd and Sc–Zr–Nb–Ta–Rh–Pd High-Entropy Alloy Superconductors on a CsCl-Type Lattice. *Chem. Mater.* **2018**, *30*, 906–914. [[CrossRef](#)]

41. Sun, L.; Cava, R.J. High-Entropy Alloy Superconductors: Status, Opportunities, and Challenges. *Phys. Rev. Mater.* **2019**, *3*, 090301. [[CrossRef](#)]
42. Werthamer, N.R.; Helfand, E.; Hohenberg, P.C. Temperature and Purity Dependence of the Superconducting Critical Field, H_{c2} . III. Electron Spin and Spin-Orbit Effects. *Phys. Rev.* **1966**, *147*, 295–302. [[CrossRef](#)]
43. Howson, M.A. Incipient Localisation and Electron-Electron Correlation Effects in Metallic Glass Alloys. *J. Phys. F Met. Phys.* **1984**, *14*, L25. [[CrossRef](#)]
44. Čulo, M.; Tafra, E.; Mihaljević, B.; Basletić, M.; Kuveždić, M.; Ivek, T.; Hamzić, A.; Tomić, S.; Hiramatsu, T.; Yoshida, Y.; et al. Hall Effect Study of the κ -(ET) $_2$ X Family: Evidence for Mott-Anderson Localization. *Phys. Rev. B* **2019**, *99*, 045114. [[CrossRef](#)]
45. Khondaker, S.I.; Shlimak, I.S.; Nicholls, J.T.; Pepper, M.; Ritchie, D.A. Two-Dimensional Hopping Conductivity in a δ -doped GaAs/Al $_x$ Ga $_{1-x}$ As Heterostructure. *Phys. Rev. B* **1999**, *59*, 4580–4583. [[CrossRef](#)]
46. Mott, S.N.F.; Davis, E.A. *Electronic Processes in Non-Crystalline Materials*; Clarendon Press: Oxford, UK, 1979.
47. Shklovskii, B.I.; Efros, A.L. *Electronic Properties of Doped Semiconductors*; Springer Series in Solid-State Sciences; Springer: Berlin/Heidelberg, Germany, 1984; Volume 45. [[CrossRef](#)]
48. Gantmakher, V.F. *Electrons and Disorder in Solids*; Oxford University Press: New York, NY, USA, 2005. [[CrossRef](#)]
49. Abeles, B.; Sheng, P.; Coutts, M.; Arie, Y. Structural and Electrical Properties of Granular Metal Films. *Adv. Phys.* **1975**, *24*, 407–461. [[CrossRef](#)]
50. Abeles, B. Granular Metal Films. In *Applied Solid State Science*; Wolfe, R., Ed.; Elsevier: Amsterdam, The Netherlands, 1976; Volume 6, pp. 1–117. [[CrossRef](#)]
51. Sheng, P. Feature Article: Electronic Transport in Granular Metal Films. *Philos. Mag. B* **1992**, *65*, 357–384. [[CrossRef](#)]

Disclaimer/Publisher’s Note: The statements, opinions and data contained in all publications are solely those of the individual author(s) and contributor(s) and not of MDPI and/or the editor(s). MDPI and/or the editor(s) disclaim responsibility for any injury to people or property resulting from any ideas, methods, instructions or products referred to in the content.